8

CELLULAR AND DENDRITIC GROWTH

Many of the alloys used in practice, such as steel, aluminum-copper alloys, nickel-base and copper-base alloys, are single phase alloys, which means that the final product of solidification is a solid solution. Depending on the thermal and compositional field, cellular or, in most practical cases, dendritic morphology will occur. In other cases, even when the room temperature microstructure is mostly eutectic some primary phases solidify before the eutectic. They can be solid solutions, carbides, intermetallic phases, inclusions, etc. Their morphology affects mechanical properties, and thus, understanding how this morphology can be controlled is a mater of significant practical importance. A detailed discussion of primary phase growth, and in particular of dendrite growth, will be provided in the following sections.

8.1 Morphology of primary phases

The interface morphology of primary phases can be classified in faceted and non-faceted. Whether a phase grows faceted or non-faceted depends mostly on its entropy of fusion. A discussion of the criterion for faceting during growth will be provided in Chapter 15, *Atomic Scale Phenomena*. At this point it is enough to state that, in general, if $\Delta S_f/R < 2$, where R is the gas constant, non-faceted growth is expected. This is mostly the case for metals. If $\Delta S_f/R > 2$, faceted growth will occur, which is common for non-metals. Some typical examples of faceted growth in metal/non-metal systems are given in Figure 8.1. The faceting behavior is also common in some transparent organic materials such as salol (Figure 8.2).

Regardless of morphology, the driving force for growth is the undercooling. Uneven undercooling on the growing surfaces of the crystal will determine dramatic changes in its morphology. A schematic sequence of the shape change of a faceted primary phase growing in the liquid from a cubic crystal to a dendrite is presented in Figure 8.3. At the corners of the cube divergent transport occurs and the thermal as well as the solutal undercooling are larger than on the facets. Consequently, the corners will grow faster, resulting in the degeneration of the cube into

a dendrite. Thus, for a faceted phase the {111} planes are the preferred growth direction.

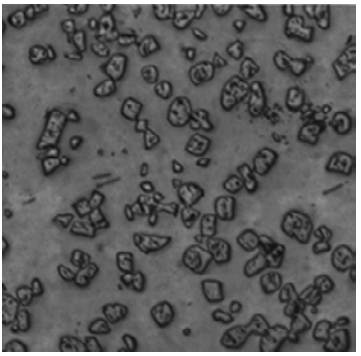

a) vanadium carbides in a Fe-C-V alloy

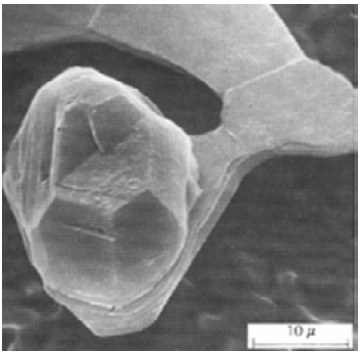

b) graphite crystal in Ni-C alloy (Lux *et a*l., 1975)

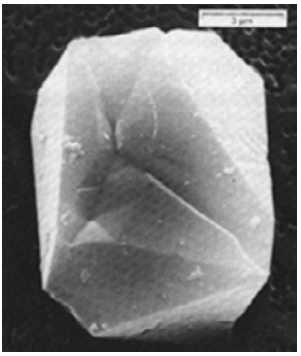

c) primary Si crystal with (111) facets in Al-Si alloy (Elliot, 1983)

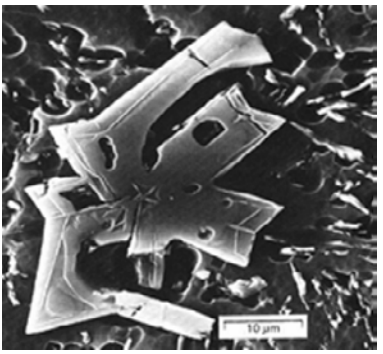

d) star-like primary Si crystal in Al-Si alloy (Elliot, 1983)

Figure 8.1. Faceted growth in metal /non-metal systems.

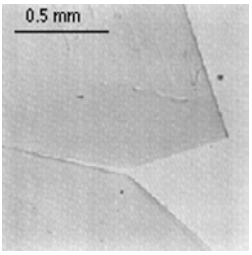

Figure 8.2. Faceted cells in salol (Hunt and Jackson, 1966).

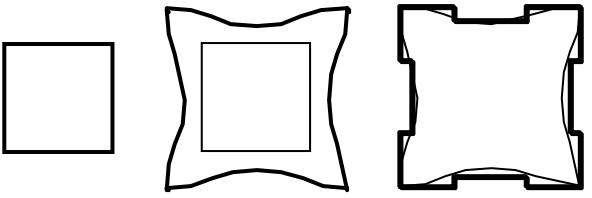

Figure 8.3. Schematic representation of the growth of a faceted dendrite.

The more interesting problem is that of the morphology of primary non-faceted phases as encountered in commercial alloys such as steel, cast iron, aluminum alloys and superalloys. At the onset of constitutional undercooling, instabilities appear on the interface as segregations associated with depressions (nodes) (Figure 8.4a). As the undercooling increases, these nodes become interconnected by interface depressions, forming first elongated cells (Figure 8.4b), and eventually a hexagonal cellular substructure (Figure 8.4c).

a) nodes b) elongated cells c) hexagonal cells

Figure 8.4. Evolution of segregation substructure as a function of constitutional undercooling; cross-section view (Biloni and Boettinger, 1970).

According to the theory of constitutional undercooling, as the undercooling increases, the cells should gradually change into dendrites. The question is how does this transition occur? Regular cells grow in the direction of heat extraction, which is typically perpendicular to the S/L interface. When the solidification velocity is increased, because of higher requirements for atomic transport, the main growth direction becomes the preferred crystallographic growth direction of the crystal (Figure 8.5a). The preferred crystallographic growth directions for some typical crystals are given in Table 8.1. At the same time with the change in growth direction, the cross section of the cell deviates from a circle to a Maltese cross, and eventually secondary arms are formed (Figure 8.5d).

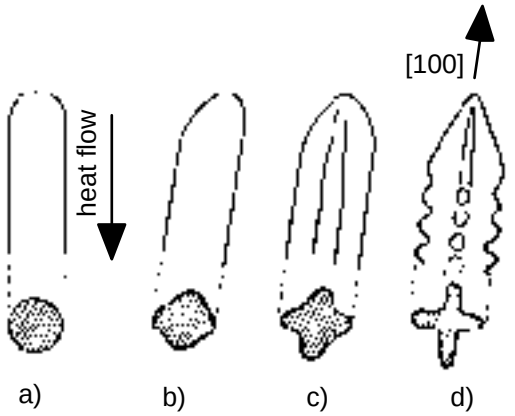

Figure 8.5. Sequential change of interface morphology as the solidification velocity increases: a) cell growing in the direction of heat extraction; b) cell growing in the [100] direction; c) cell /dendrite; d) dendrite (Morris and Winegard, 1969). Reprinted with permission form Elsevier.

The preferred crystallographic growth directions for some typical crystals are given in Table 8.1. The orientation of the growing dendrite with respect to the direction

of the heat flow can affect significantly the dendrite morphology, as exemplified in Figure 8.6.

Table 8.1. Preferred crystallographic growth directions.

Crystal structure	Growth direction	Example
fcc	[100]	Al
bcc	[100]	δFe
bc tetragonal	[110]	Sn
hcp	$[10\bar{1}0]$	ice flakes, graphite
	[0001]	$Co_{17}Sm_2$

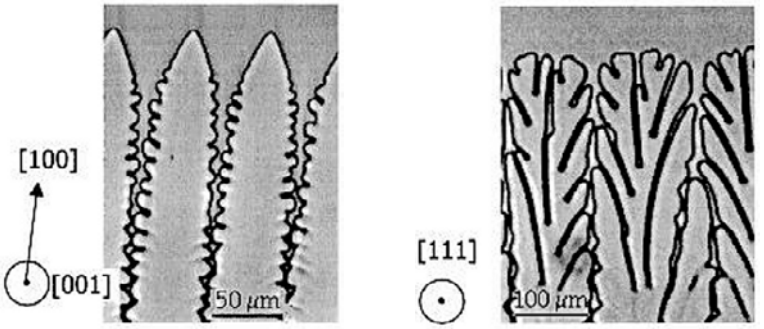

Figure 8.6. Effect of crystalline anisotropy on the morphology of directionally solidified dendrites; growth velocity 35μm/s, heat extraction upward; thin films of a CBr_4–8mol% C_2Cl_6 alloy (Akamatsu *et al*., 1995).

8.2 Analytical tip velocity models

Cells are a relatively simple periodic pattern of the S/L interface. Dendrites that evolve during solidification of metals are complex patterns characterized by side branches (primary, secondary, tertiary, etc.). Describing mathematically the temporal evolution of such patterns is a challenging endeavor. Both analytical and numerical models have been proposed to describe dendritic growth. Only analytical models will be discussed in this chapter.

The analytical models are limited in scope, attempting to describe solely dendrite tip kinetics, as determined by the thermal and solutal field, and by capillarity. Dendritic array models include also an analysis of transport from the root to the tip.

8.2.1 Solute diffusion controlled growth (isothermal growth) of the dendrite tip

Consider a needle-like crystal growing in the liquid. Assume diffusion-controlled growth, which means that the only driving force for growth is the concentration gradient (curvature and thermal undercooling ignored).

In a first approximation, let us assume that the tip of the crystal is a hemi-spherical cap (hemi-spherical approximation), as shown in Figure 8.7. Flux balance at the interface gives:

$$\pi r^2 V\left(C_L - C_S\right) = -2\pi r^2 D\left(\frac{dC}{dr}\right)_{tip} \quad \text{or} \quad VC_L\left(1-k\right) = -2D\left(\frac{dC}{dr}\right)_{r=r_o} \tag{8.1}$$

The solution of this equation is (see inset for derivation):

$$P_c = \Omega_c \tag{8.2}$$

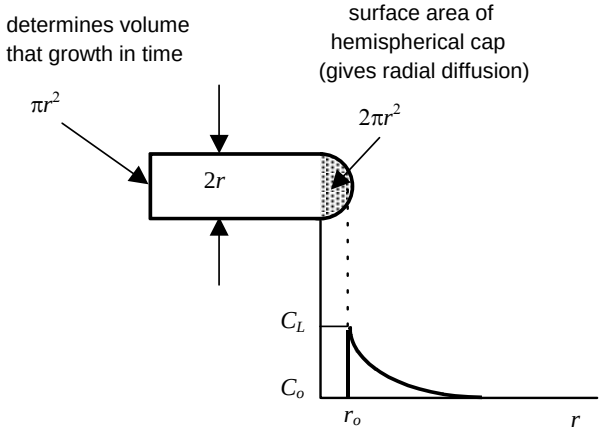

Figure 8.7. Diffusion field ahead of a hemispherical needle.

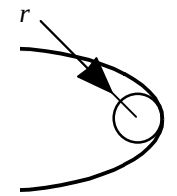

Figure 8.8. Dendrite tip having the shape of a paraboloid of revolution.

where the solutal Péclet number as defined earlier is:

$$P_c = V\,r/2D \tag{8.3}$$

and the solutal supersaturation, Ω_c, is given by Eq. (7.18). Substituting in Eq. (8.2) we obtain:

$$V = 2D_L\,\Omega_c/r \tag{8.4}$$

Derivation of the growth velocity of the hemispherical needle, Eq. (8.2).
To find the composition gradient at the tip of the crystal it is necessary to solve the steady state diffusion equation in radial coordinates with no tangential diffusion:

$$\frac{d^2C}{dr^2} + \frac{2}{r}\frac{dC}{dr} = 0 \quad \text{or} \quad r^2\frac{d^2C}{dr^2} + 2r\frac{dC}{dr} = 0 \quad \text{or} \quad \frac{d}{dr}\left(r^2\frac{dC}{dr}\right) = 0$$

The general solution of this equation is $C = C_1 + C_2/r$, where C_1 and C_2 are constants. The following boundary conditions are used:

at $r \to \infty$	$C = C_o$	thus	$C_1 = Co$
at $r = r_o$	$C = C_L$	thus	$C_2 = r_o\,(C_L - C_o)$

Then:

$$\left(\frac{dC}{dr}\right)_{r=r_o} = \left[-\frac{r_o}{r^2}\left(C_L - C_o\right)\right] = -\frac{C_L - C_o}{r_o}$$

Substituting in Eq. (8.1) we obtain: $\dfrac{V\,r_o}{2D} = \dfrac{C_L - C_o}{C_L\left(1-k\right)}$, and since the solutal supersaturation is $\Omega_c = \left(C_L - C_o\right)/\left[C_L\left(1-k\right)\right]$ and the solutal Péclet number is $P_c = V\,r_o/\left(2D\right)$ we obtain the final solution Eq. (8.2).

Eq. (8.4) gives the growth velocity of the hemispherical needle. It indicates that velocity depends on tip radius, r, and on supersaturation, Ω_c, which is the driving force. However, velocity is not uniquely defined since this equation does not have a unique solution for V, but rather pairs of solutions for V and r. In other words, the solution of the diffusion equation does not specify whether a dendrite will grow fast or slow, but only relates the tip curvature to the dendrite rate of propagation.

The other problem with this solution is that the shape defined by this velocity is not self-preserving. In other words, the hemispherical cap does not grow only in the x-direction, but also in all r-directions, meaning that the needle thickens as it grows. Experimental work on dendrite growth has demonstrated that the dendrite tip preserves its shape. Consequently, another solution must be found for the diffusion problem.

If it is assumed that the dendrite tip has the shape of a paraboloid of revolution (Figure 8.8), which is self-preserving, the solution to the steady state diffusion equation given by Ivantsov (1947) is:

$$\mathrm{I}(P_c) = \Omega_c \quad \text{where} \quad \mathrm{I}\left(P_c\right) == P_c\exp(P_c)\,E_1(P_c) = P_c\exp\left(P_c\right)\int_P^\infty \frac{\exp(-x)}{x}\,dx \qquad (8.5)$$

Here, $E_1(P_c)$ is the exponential integral function. This solution is valid for both the solutal diffusion (P_c and Ω_c) and the thermal diffusion (P_T and Ω_T).

There are several approximations of the Ivantsov number, I(P), that can be used in numerical or analytical calculations (see inset). Since I(P) is a function of both V and r, the problem of evaluating an unique velocity is still to be solved.

Approximation of the Ivantsov number.

$$\mathrm{I}(P) = \cfrac{P}{P + \cfrac{1}{1 + \cfrac{1}{P + \cfrac{2}{1 + \cfrac{2}{P + \ldots}}}}}$$

The continued fraction approximation is:

Note that the zero-th approximation of the continued fraction approximation of the Ivantsov function is $I_0(P) = P$, that is the hemispherical approximation.

Typically, for casting solidification $P < 1$. For this case the following approximation can be used (Kurz and Fisher, 1989):

$$I(P) = P\cdot\exp(P)\cdot[a_o + a_1\cdot P + a_2\cdot P^2 + a_3\cdot P^3 + a_4\cdot P^4 + a_5\cdot P^5 - \ln(P)]$$

where a_o = -0.57721566, a_1= 0.99999193, a_2= -0.24991055, a_3= 0.05519968, a_4= -0.00976004, a_5= 0.00107857.

For limiting values of the Péclet number, the Ivantsov function for a paraboloid of revolution can be approximated as (Trivedi and Kurz, 1994):

for $P<<1$: $I(P) \approx -P\ln P - 0.5772\,P$
for $P>>1$: $I(P) \approx 1 - 1/P + 2/P^2$

8.2.2 Thermal diffusion controlled growth

During solidification, a thermal gradient is imposed over the system. Thermal diffusion will drive the process. In pure metals, this will be the only driving force for growth. If it is assumed that the driving force for perturbation growth is only the thermal gradient (thermal dendrite), similar equations to those obtained for the diffusion-controlled growth can be derived:

$$P_T = \Omega_T \quad \text{with} \quad P_T = \frac{Vr}{2\alpha} \quad \text{and} \quad \Omega_T = \frac{\Delta T_T}{\Delta H_f / c} \tag{8.6a}$$

and alternatively:

$$I(P_T) = \Omega_T \tag{8.6b}$$

where P_T is the thermal Péclet number and Ω_T is the thermal supersaturation. For the hemispherical approximation a derivation of the particular case of Eq. (8.6b) is given in the inset.

Derivation of the correlation between the thermal Péclet number and thermal supersaturation.

Temperature flux balance at the interface gives: $\pi r^2 V \frac{\Delta H_f}{c} = -2\pi r^2 \alpha_L \left(\frac{dT}{dr}\right)_{r=r_o}$

To calculate the thermal gradient at the interface we need the temperature of the tip. The solution of the steady state diffusion equation in radial coordinates is $T = C_1 + C_2/r$. Applying the boundary conditions: i) at $r \to \infty$ - $T = T_{bulk}$ and ii) at $r = r_o$ - $T = T_f$, the solution becomes $T = T_{bulk} + \Delta T\cdot r_o/r$.

Thus, the temperature gradient at the tip is $\left(dT/dt\right)_{r=r_o} = -\Delta T_T / r_o$. Substituting in the flux balance equation and rearranging:

$$\frac{Vr}{2\alpha} = \frac{\Delta T_T}{\Delta H_f / c} \quad \text{or} \quad P_T = \Omega_T$$

All the diffusion models discussed above conclude that at steady state, the tip of the dendrite will advance in the liquid following the simple law $V \cdot r$ = const. This means that there is no unique solution, since multiple pairs of V and r satisfy this relationship. However, experimental work has demonstrated that for each undercooling a unique value of tip velocity and radius is obtained. The problem is then to find the additional constrains that impose a unique dendrite tip radius from the multiple solutions offered by the diffusion models.

8.2.3 Solutal, thermal, and capillary controlled growth

To obtain a unique solution it is necessary to find additional criteria that define the tip radius. Several models have been proposed:

- the *extremum* criterion
- the marginal stability criterion
- the microsolvability theory

The *extremum* criterion

As discussed earlier, at high solidification velocities, when the diffusion length becomes of the size of the solute capillary length ($D/V = \Gamma/\Delta T_o$), the interface becomes planar. Thus, as shown in Figure 8.9, the maximum velocity of a dendrite tip is limited by the absolute stability. The *extremum* criterion implies that the perturbation will grow at the maximum possible velocity and the minimum possible undercooling. These conditions are satisfied by the velocity corresponding to the radius tip of the dendrite r_e.

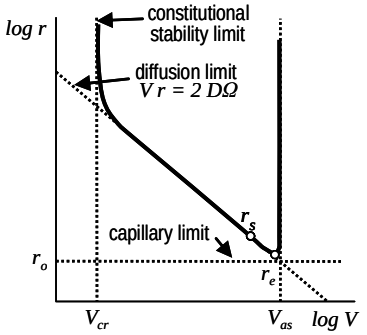

Figure 8.9. Growth velocity - tip radius correlation; the full line is the *V-r* correlation.

An expression for V can be obtained for example for a perturbation driven only by the solutal and curvature undercooling (solutal perturbation), starting from:

$$\Delta T = \Delta T_c + \Delta T_r$$

where

$$\Delta T_c = -m(C_L - C_o) = -m(C_L - C_S)\Omega_c = -m(1-k)C_L\Omega_c = m(k-1)C_L P_c = -m(1-k)C_L \frac{Vr}{2D} \quad \text{and} \quad \Delta T_r = \frac{2\Gamma}{r} \tag{8.7}$$

Substituting these last two equations in the total undercooling equation we have:

$$\Delta T = -m(1-k)C_L^* \frac{Vr}{2D} + \frac{2\Gamma}{r} \tag{8.8}$$

According to the *extremum* criterion, it will be assumed that growth proceeds at the minimum undercooling (the maximum of the curve) which can be obtained from $\partial \Delta T / \partial r = 0$, that is:

$$r_e = \left[\frac{4D\Gamma}{m(k-1)C_L^*}\right]^{1/2} V^{-1/2} = \sqrt{\frac{4\Gamma}{G_L}} \tag{8.9}$$

Substituting in Eq. (8.8) an equation for tip velocity is obtained:

$$V = \mu \Delta T^2 \quad \text{with} \quad \mu = \frac{D_L}{4\Gamma m(k-1)C_L^*} \tag{8.10}$$

Note that for steady state solidification, $C_L^* = C_o / k$.

However, experimental evidence (Nash and Glicksman, 1974) demonstrates that such velocities are considerable higher than the measured ones. This is shown schematically in Figure 8.9, where r_s is the position of the experimental point and r_e is the value calculated from the *extremum* criterion.

The marginal stability criterion

Langer and Müller-Krumbhaar (1978) performed a linear stability analysis for an Ivantsov parabola dendrite tip region in a pure undercooled melt. A small departure from the parabolic shape, caused by interface energy, was introduced in the system. It was concluded that dendrite tip radii are not stable at values smaller than predicted by the extremum criterion, or larger than a certain critical value. At such large radii tip splitting will occur to decrease the radius. They proposed that this largest radius is selected by the dendrite during its growth (*marginal stability* criterion). A number of models discussed in the following paragraphs use this criterion to obtain a unique dendrite tip radius.

To formulate the growth velocity of the dendrite tip for the most general case it is assumed that the tip is a growth instability driven by the kinetic, solutal, thermal, and capillary undercooling:

$$\Delta T = \Delta T_k + \Delta T_c + \Delta T_T + \Delta T_r \tag{8.11}$$

A comprehensive treatment of this problem applicable to a wide range of Péclet numbers was given by Boettinger *et al.* (1988). ΔT_k was formulated through Eq. 2.26, ΔT_T through Eq. (8.6a), and ΔT_r as $2\Gamma/r$. The constitutional undercooling was written as:

$$\Delta T_c = -m_L(V)\left(C_L - C_o\right) = m_L C_o\left[1 - \frac{m_L(V)/m_L}{1-\left(1-k_e\right)\Omega_c}\right] \tag{8.12}$$

Here, $m_L(V)$ is the velocity dependent liquidus slope given in Eq. 2.32. When all these equations are introduced in Eq. (8.11), the values of dendrite tip velocity and tip radius for a given ΔT can be calculated. A dependency as shown in Figure 8.9 is obtained. To obtain a unique value for dendrite tip velocity it was assumed that growth occurs at the limit of stability (marginal stability criterion). In other words, the perturbation will grow with the shortest stable wavelength, *i.e.*, $r_s = \lambda_i$. This implies that if the tip radius of the perturbation is smaller than λ_i, the radius will tend to increase, while if it is larger than λ_i, additional instabilities will form and the radius will decrease. Then, for $\dot{\varepsilon}/\varepsilon = 0$, Eq. (7.23) gives:

$$r^2 = \frac{\Gamma/\sigma^*}{G_L\,\xi_c - G_T\,\xi_T} \quad \text{with} \quad \sigma^* = \left(4\pi^2\right)^{-1} \tag{8.13}$$

Note that this equation can be used to derive dendrite growth velocity equations for both slow solidification rates typical for castings (P<1) and rapid solidification rates (P>>1). The modified Eq. (8.11) and Eq. (8.13) can now be concomitantly solved numerically to give a unique solution for the dendrite tip velocity.

In their model, Lipton *et al.* (1984) also started from Eq. (8.11), ignored the kinetic undercooling, and used the formulations for ΔT_c, ΔT_T, andΔT_r as before:

$$\begin{aligned}\Delta T &= \Delta T_T + \Delta T_c + \Delta T_r \\ &= \frac{\Delta H_f}{c_p} I(P_T) + mC_o\left[1 - \frac{1}{1-(1-k)\,I(P_c)}\right] + \frac{2\Gamma}{r}\end{aligned} \tag{8.14}$$

The dendrite tip radius is derived form the marginal stability theory as:

$$r = \frac{\Gamma}{\sigma^*}\left[\frac{\Delta H_f}{c_p} P_T - P_c \frac{mC_o(1-k)}{1-(1-k)\,I(P_c)}\right]^{-1} \tag{8.15}$$

From the solution of the diffusion field the tip velocity is formulated as:

$$V = 2\alpha P_T/r \tag{8.16}$$

Finally, the solutal and thermal Péclet numbers are correlated by:

$$P_c = P_T\,(\alpha/D) \tag{8.17}$$

Here, σ^* is the dendrite tip selection parameter $\approx 1/(4\pi^2)$. This parameter will be discussed later in more detail. Since velocity is introduced through the thermal and solutal supersaturations, either the hemispherical ($P = \Omega$) or the paraboloid (I(P) = Ω) approximations can be used.

The dendrite tip velocity for equiaxed dendrites growing at small undercooling can be calculated from the preceding four equations which are solved by numerical iterations.

A more complete solution was derived by Trivedi and Kurz (1994). They started with Eq. (8.11) and obtained an equation similar to Eq. (8.14), but with a different formulation for the solutal undercooling (second RH term) as follows:

$$\Delta T_c = \frac{k\,\Delta T_o\, I(P_c)}{1-(1-k)\,I(P_c)} \tag{8.18}$$

The capillary term in Eq. (8.14) is generally negligible for metals at low undercooling (the case of shaped castings), but is significant under rapid solidification conditions. Substituting the values for the thermal and constitutional gradients in (8.13), the general dendrite tip radius selection criterion in undercooled alloys is obtained:

$$Vr^2\left(\frac{k_V\,\Delta T_o(V)}{\Gamma\, D}\right)\left(\frac{1}{1-(1-k_V)\,I(P_c)}\right)\xi_c + Vr^2\left(\frac{\Delta H_f/c_L}{2\Gamma\,\alpha_L\,\beta}\right)\xi_L = \frac{1}{\sigma^*} \tag{8.19}$$

where $\Delta T_o(V)$ is the velocity dependent solidification interval and $\beta = 0.5[1 + (k_S/k_L)]$. This equation is valid for slow as well as rapid cooling unconstrained growth. The modified Eq. (8.14) and Eq. (8.19) completely describe the dendrite growth problem and can be solved numerically to obtain the growth velocity.

A simple analytical solution can be obtained for a solutal dendrite under the assumption of small Péclet number ($P_c = 0$, $\xi_c = 1$):

$$V\,r^2 = \frac{4\pi^2\Gamma\, D_L}{m(k-1)C_o} \tag{8.20}$$

For constrained growth (directional solidification) they proposed the equation:

$$V\left(\frac{k\,\Delta T_o}{D}\right)\left(\frac{C_L^*}{C_o}\right)\xi_c - G_T = \frac{\Gamma}{\sigma^*\, r^2} \tag{8.21}$$

Purely analytical solutions can be obtained with further simplifying assumptions. Following the derivation proposed by Nastac and Stefanescu (NS) (1993) for unconstrained growth (equiaxed dendrites), ignoring kinetic undercooling and assuming that the effect of surface energy (curvature) is introduced through the limit of stability criterion, only the solutal and thermal undercooling must be considered. The dendrite tip velocity equation is (see inset for derivation):

$$V = \mu_{eq}\,\Delta T^2 \quad \text{with} \quad \mu_{eq} = \left[2\pi^2 \Gamma \left(\frac{m(k-1)C_L^*}{D_L} + \frac{\Delta H_f}{c\alpha_L} \right) \right]^{-1} \tag{8.22}$$

The growth coefficient can also be written as:

$$\mu_{eq} = \left(\mu_c^{-1} + \mu_T^{-1} \right)^{-1} \quad \text{with} \quad \mu_c = \frac{D_L}{2\pi^2 \Gamma m(k-1) C_L^*} \quad \text{and} \quad \mu_T = \frac{c\alpha_L}{2\pi^2 \Gamma \Delta H_f}$$

For steady state, C_L^* will be substituted with C_o/k. The growth coefficient is a constant only for steady state, since C_L^* is constant only for steady state. An equation similar to Eq. (8.22) can be obtained if a paraboloid of revolution shaped tip is assumed. Then, the I(P) = Ω relationships must be used in the derivation.

This equation describes unconstrained growth (equiaxed dendrites) since it includes thermal undercooling ahead of the interface. For some metallic alloys, it can be calculated that the contribution of thermal undercooling is negligible as compared to that of solutal undercooling (see Application 8.1). Then, the velocity equation can be simplified. Since $\Delta T_T = 0$ and thus $G_T = 0$, tip velocity is given by Eq. (8.22) with the growth coefficient given by the equation for μ_c.

Derivation of the Nastac-Stefanescu equation.
When using the assumptions used by the model the total undercooling is:

$$\Delta T = \Delta T_c + \Delta T_T \tag{8.23}$$

where ΔT_c is given by Eq. (8.7) and ΔT_T is calculated from Eq. (8.6a). If it is further assumed that the tip of the instability is of hemispherical shape, and substituting the value of P_c and $P_T = \Omega_T$ it is obtained that:

$$\Delta T = \frac{Vr}{2} \left(\frac{m(k-1)C_L^*}{D_L} + \frac{\Delta H_f}{c\alpha_L} \right) \tag{8.24}$$

The liquidus and thermal gradients are:

$$G_L = -m\frac{\partial C_L}{\partial r} = \frac{V}{2D_L} m C_L^* (k-1) = \frac{P_c}{r}\frac{\Delta T_c}{\Omega_c} = \frac{\Delta T_c}{r}$$

$$G_T = -\frac{\partial T_T}{\partial r} = -\frac{V}{2\alpha_L}\frac{\Delta H_f}{c} = -\frac{P_T}{r}\frac{\Delta T_T}{\Omega_T} = -\frac{\Delta T_T}{r}$$

The first of these two equations was obtained from Eq. (4.5). A factor of ½ was introduced to describe the flux at the hemispherical tip. The last equation is valid for a negative gradient, which occurs during equiaxed solidification. Then, assuming that growth occurs at the limit of stability ($r = \lambda_i$), Eq. (7.26) gives $r = 2\pi\sqrt{\Gamma/(G_L - G_T)}$. Substituting the expressions for G_L and G_T, and using Eq. (8.23) the tip radius is:

$$r = 4\pi^2\Gamma/\Delta T \tag{8.25}$$

Substituting this expression for r in Eq. (8.24) the equation for the hemispherical tip velocity, Eq. (8.22), is obtained.

For the case of columnar dendrites (constrained growth), there is no thermal undercooling. Thus, ignoring the kinetic undercooling, the basic undercooling equation simplifies to $\Delta T = \Delta T_c + \Delta T_r$.

Using similar formulations for the undercooling as above, and the hemispherical approximation, Kurz, Giovanola, and Trivedi (KGT) (1986) derived the following equation for columnar dendrites:

$$V = \frac{m(k-1)C_o D_L \Omega_c^2}{\pi^2\Gamma} = \frac{D_L}{\pi^2\Gamma m(k-1)C_o}\Delta T_c^2 \tag{8.26}$$

Both the KGT and NS models are only valid for small Péclet numbers, since this assumption was used to derive Eq. (7.27), which is adopted for the limit of stability criterion.

Let us now evaluate to what degree the simplifications introduced in the analytical Nastac-Stefanescu (NS) model produce deviations from the more accurate semi-analytical Trivedi-Kurz (TK) model. To this effect, a comparison of calculated *V-r* correlations with the two models and experimental data is shown in Figure 8.10 (for details of the calculation see Application 8.3). Both models are very close to the experimental data on the linear part of the log-log graph. As the growth velocity decreases and a dendritic-to-cellular transition occurs, the radius increases very fast (it should tend to infinity when planar solidification occurs). Only the TK model for columnar growth (simplified Eq. (8.20)) follows well the experimental data in the velocity range smaller than 1μm/s. However, as typical velocities in casting solidification are in the range of 0.01 to 0.5m/s, it is apparent that both models can be used.

A columnar dendrite operates in a constrained environment, since the temperature gradient ahead of the interface is always positive. Its growth is driven by the temperatue gradient. The interface temperature of the columnar dendrite is between T_L and T_S, and the undercooling is mostly constitutional, ΔT_c. The assumption of negligible thermal undercooling is reasonable for most metallic alloys, so that its growth velocity can be calculated with $V_c = \mu_c \Delta T_c^2$. At steady state the columnar

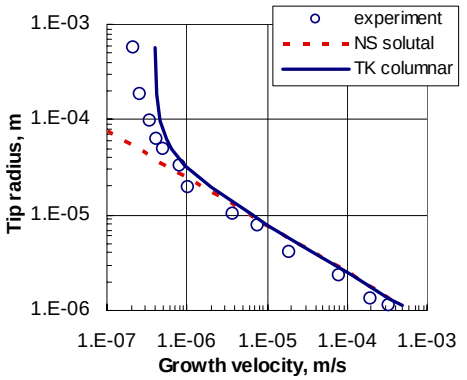

Figure 8.10. Measured and calculated tip radii of cells and dendrites in a Fe-3.08%C-2.01%Si alloys solidified under a thermal gradient of 5000K/m at various velocities. Experimental data are from Tian and Stefanescu (1992).

dendrite can grow at a maximum velocity corresponding to the maximum undercooling $\Delta T_c = \Delta T_o$. However, steady state can be reached also at an undercooling smaller than ΔT_o, when the solutal velocity, V_c, is equal to the thermal velocity, V_T, calculated from macro-transport considerations. As long as $V_c < V_T$, the tip velocity is simply V_c. If, on the contrary, $V_c > V_T$, dendritic growth is constrained at V_T.

An equiaxed dendrite operates in an unconstrained environment, since the temperature gradient ahead of the interface is negative. Its velocity is again mostly dictated by the constitutional undercooling, and can be calculated with Eq. (8.22), as long as $\Delta T_{bulk} < \Delta T_o$ (see example in Application 8.5). If $\Delta T_{bulk} > \Delta T_o$ ($T^* < T_S$), then, interface equilibrium does not apply anymore, and the partition coefficient is velocity dependent.

Koseki and Flemings (1995) developed a model that includes the combined effects of the undercooled melt and heat extraction through the solid, applicable to chill-casting. It is a hybrid of the models for constrained and unconstrained growth.

Experimental work by Nash and Glicksman (1974) has demonstrated that, indeed, the operating point of the dendrite is close to the value calculated from the limit of stability criterion (r_s on Figure 8.9). In their experiment, they measured concomitantly r, V, and ΔT during the growth of a succinonitrile dendrite. It was also proven that the tip of the dendrite fits a parabolic curve (dotted line on Figure 8.11).

The microsolvability theory

While, as discussed, the marginal stability criterion gives an excellent agreement with most experimental results, there is no physical reason to accept the marginally stable state over the other stable states.

Kessler and Levine (1986) and Bensimon *et al.* (1987) have found a unique, self-consistent solution to the steady-state dendrite problem (the interface shape obtained from the thermal and solutal field equations with the boundary conditions that includes the effect of surface energy satisfies the shape preserving condition) taking into account the anisotropy of the interface energy around the dendrite tip. This unique solution, known as the microsolvability condition, gives a unique value for the dendrite tip radius.

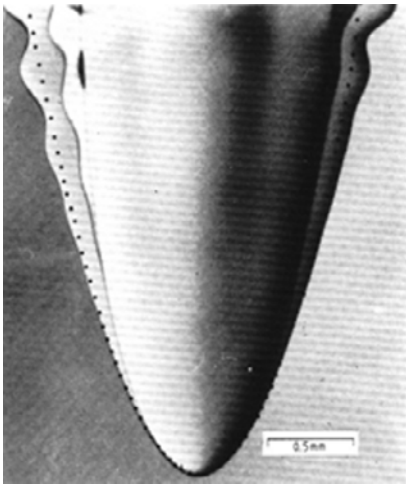

Figure 8.11. Tip of a growing succinonitrile dendrite (Huang and Glicksman, 1981). Reprinted with permission from Elsevier.

The concept that the capillary effect is a singular perturbation which destroys Ivantsov's continuous family of solutions has been confirmed by analytical and numerical studies. While the solvability theory has achieved notable theoretical successes, its quantitative relevance to the interpretation of experimental data has not been established (Barbieri and Langer, 1989).

8.2.4 Interface anisotropy and the dendrite tip selection parameter σ^*

In their analysis, Langer and Müller-Krumbhaar (1978) introduced the dendrite tip selection parameter, σ^* through the relationship:

$$r = \left(\delta_c \, d_o / \sigma_c^*\right)^{1/2} \tag{8.27}$$

where $\delta_c = 2D_L/V$ is the diffusion length, $d_o = \Gamma/\Delta T_o$ is the capillary length, and σ^*_c is the parameter for the solutal case (with $D_S << D_L$). Substituting these relationships this equation can be rewritten as:

$$V r^2 = 2\Gamma D / \left(\sigma_c^* \, \Delta T_o\right) \tag{8.28}$$

Note that this equation is identical with Eq. (7.29) when assuming $\lambda_i = r$, and using the notation $\sigma^* = 1/4\pi^2$. In the marginal stability theory this parameter is considered to be a constant equal to 0.02533.

Similarly, a parameter for the purely thermal case (for $\alpha_S = \alpha_L$) can be derived, using for example Eqs. (8.6a) and (8.25), to obtain:

$$\frac{1}{\sigma_T^*} = V r^2 \left(\frac{\Delta H_f / c_L}{2\Gamma \alpha_L} \right) \tag{8.29}$$

In order to analyze the dendrite tip selection parameter for undercooled alloys, Trivedi and Kurz (1994) substituted Eqs. (8.28) and (8.29) in Eq. (8.19) to obtain:

$$\left(\frac{2}{\sigma_c^*}\right)\left(\frac{C_L^*}{C_o}\right)\xi_c + \left(\frac{1}{\sigma_T^*}\right)\left(\frac{\xi_L}{\beta}\right) = \frac{1}{\sigma^*} \tag{8.30}$$

They stated that for an alloy system, σ^* is constant, but σ_c^* and σ_T^* are not.

The microsolvability theory produces equations similar in form as those derived through the marginal stability criterion. The main difference is that σ^* is not a numerical constant any more, but rather a function of the interface energy anisotropy parameter, ε, as follows:

$$\sigma^* = \sigma_o \, \varepsilon^{1.75} \tag{8.31}$$

where σ_o is of the order of unity and the definition of ε is discussed in the following paragraphs.

Crystalline materials are characterized by anisotropic S/L interface energy. For cubic crystals, the variation of the interfacial energy γ with orientation θ can be expanded about the dendrite tip orientation ($\theta = 0$), which has four-fold symmetry. This expansion up to the first order term is (Trivedi and Kurz, 1994) $\gamma(\theta) = \gamma_o(1 + \delta \cos 4\theta)$, where δ is the interface anisotropy parameter.

Using the Gibbs-Thomson equation for anisotropic materials, the capillary undercooling is:

$$\Delta T_r = \left(\gamma + d^2\gamma / d\theta^2\right) K / \Delta S_f = \gamma_o \left(1 - \varepsilon \cos 4\theta\right) K / \Delta S_f \tag{8.32}$$

where $\varepsilon = 15\delta$ and is known as the anisotropy coefficient.

The anisotropy in the S/L interface energy strongly affects the tip radius. Higher anisotropy reduces the tip radius (Lu and Liu, 2007).

8.2.5 Effect of fluid flow on dendrite tip velocity

The rather intricate picture of dendritic growth presented so far is made even more complicated by buoyancy-driven convection, which is unavoidable during solidification under terrestrial conditions. It was calculated (Miyata, 1995) that the growth velocity of the dendrite increases with the forced melt flow at a given undercooling. The effect of melt flow becomes particularly significant in the low velocity regime of both dendrite growth and forced flow.

For the case of uniform fluid velocity, u_∞, directed opposite to the crystal growth direction, Ananth and Gill (1991) have proposed a simplified approximation for the effect of fluid flow on the velocity-undercooling relation. Their solution of the three-dimensional Navier-Stokes equation under the approximation of low Reynolds number, Re, resulted in the following expression for the thermal melt undercooling:

$$\Delta T_t = \frac{u_\infty r \Delta H_f}{2\alpha c_L} \int_1^\infty \exp\left[-\int_1^z f(\eta)\, d\eta \right] dz$$

with the function $f(\eta)$ given by:

$$f(\eta) = \frac{r}{2\alpha}(u_\infty + V) + \frac{1}{\eta} - \frac{V r \left(\exp\left[-Re^*/2\right] - \exp\left[-Re^* \eta/2\right]\right)}{Re^* \eta \alpha E_1\left(Re^{*}/2\right)} - \frac{V r E_1\left(Re^* \eta/2\right)}{2\alpha E_1\left(Re^*/2\right)}$$

Re^* is defined by the relation $Re^* = V r/\nu + Re$, with the Reynolds number $Re = u_\infty r/\nu$. E_1 denotes the exponential integral function and ν is the kinematic viscosity.

Glicksman *et al*. (1995) measured the dendritic growth velocities and tip radii of succinonitrile in micro-gravity environment experiments (space shuttle Columbia) during isothermal solidification (Figure 8.12). It was observed that convective effects under terrestrial conditions increase the growth velocity by a factor of two at lower undercoolings (< 0.5K). In the undercooling range of 0.47 to 1.7K, the data remained virtually free of convective effects. A diffusion solution to the dendrite problem was not consistent with the experimental data.

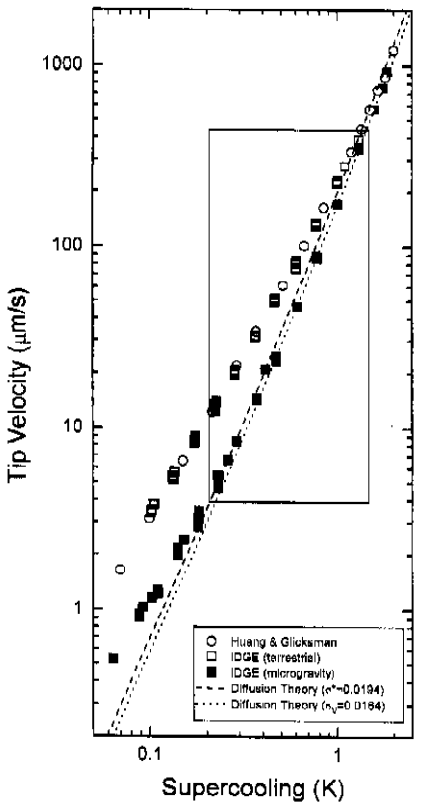

Figure 8.12. Dendrite tip velocity as a function of undercooling for terrestrial and microgravity conditions (Glicksman *et al*., 1995).

8.2.6 Multicomponent alloys

Eq. (8.22) can be extended to dilute multicomponent systems, by writing the growth constant as (Nastac and Stefanescu, 1993):

$$\mu = \frac{1}{2\pi^2}\left[\sum_{i=1}^{n}\left[\Gamma_i\left(\frac{m_i(k_i-1)C_{Li}^{*\,2}\rho_i}{D_{Li}\sum_{j=1}^{n}C_{Lj}^{*}\rho_j}+\frac{\Delta H_f}{c\alpha_L}\right)\right]\right]^{-1} \tag{8.33}$$

where *i* is the component, and *n* is the number of components in the alloy that have a significant contribution upon the tip growth velocity.

The solidification parameters of interest for modeling for calculation of dendrite tip velocity of multicomponent alloys, *i.e.*, the equilibrium liquidus temperature, T_L, the liquidus slope, m_L, and the partition coefficient, k, can be obtained by using thermodynamic calculation, as described by Boettinger *et al.* (1988). However, when these parameters are used one needs to solve the mass transport equation for each species.

To avoid excessive computational time a combined multicomponent/pseudobinary approach can be used (Nastac *et al.*, 1999). First, thermodynamic calculations are used to obtain the slope of the liquidus line and the partition coefficient for each element at successive temperatures. The algorithm for such calculations is now incorporated in some solidification simulation software (*e.g.*, the SLOPE subroutine in ProCAST). Then, an equivalent slope, $\overline{m}_L$, and partition coefficient, $\overline{k}$, are calculated for each temperature using the equations:

$$\overline{m}_L = \frac{\sum_{i=1}^{n}\left(m_L^i C_L^i\right)}{\overline{C}_L} \quad \text{and} \quad \overline{k} = \frac{\sum_{i=1}^{n}\left(m_L^i C_L^i k^i\right)}{\sum_{i=1}^{n}\left(m_L^i C_L^i\right)}$$

where $\overline{C}_L$ is the sum of all the elements in the liquid, and m_L^i, C_L^i, and k_L^i are the slope, liquid composition, and partition coefficient of individual elements, respectively. Then regression equations were fitted through the m_L-T and k_L-T curves to obtain the temperature dependence of m_L and of k_L:

$$\overline{m}_L = a + b\cdot T + c\cdot T^2 \quad \text{and} \quad \overline{k} = a' + b'\cdot T + c'\cdot T^2$$

where *a*, *b*, etc., are known coefficients.

The liquidus temperature can be calculated using the equivalent slope:

$$T_L = T_f + \overline{m}_L \cdot \overline{C}_L$$

or from the weighted average of the slope and liquid composition of each element:

$$T_L = T_f + \sum_i m_L^i \, C_L^i$$

where T_f is the melting temperature of the pure solvent.

8.3 Dendritic array models

In the preceding discussion only events happening around the tip have been considered. However, most practical interest resides in structures that are the result of the growth of arrays of instabilities. In this case lateral diffusion and diffusion from the root to the tip of the instability must also be included.

Bowers *et al.* (1966) proposed a model in which the contribution of liquid diffusion from root to tip was included (Figure 8.13). Solute balance in the volume element is:

$$D_L \frac{\partial}{\partial x}\left(f_L \frac{\partial C_L}{\partial x} \right) = \frac{\partial \overline{C}}{\partial t}$$

where $\overline{C}$ is the average composition of the volume element at time t. The variation of composition in time is:

$$\frac{\partial \overline{C}}{\partial t} = C_L (1-k) \frac{\partial f_L}{\partial t} + f_L \frac{\partial C_L}{\partial t}$$

The first term on the right hand side is the solute rejected from the growth of the perturbation (growth in x and y-directions). The second term is the solute entering the volume element due to liquid phase diffusion from root to tip (x-direction). The governing equation becomes:

$$\frac{\partial}{\partial x}\left(D_L \, f_L \frac{\partial C_L}{\partial x} \right) = C_L (1-k) \frac{\partial f_L}{\partial t} + f_L \frac{\partial C_L}{\partial t} \tag{8.34}$$

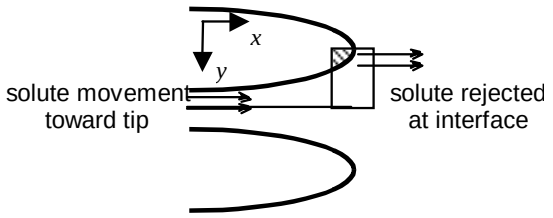

Figure 8.13. Array of instabilities.

For steady-state solidification, solute flux balance at the tip gives $V(C_t - C_o)_{tip} = -D_L(\partial C/\partial x)_{tip}$. For constant concentration gradient along *x* between perturbations from root to tip the concentration gradient is $\partial C/\partial x = = -m^{-1}\, dT/dx = G/m$. Substituting this gradient in the previous equation, the tip composition is obtained as:

$$C_t = (1 - a)\, C_o \quad \text{with} \quad a = D_L G_L/(m V C_o) \tag{8.35}$$

The composition gradient at the interface can then be expressed as:

$$\frac{\partial C}{\partial x} = \frac{V}{D}(C_L - C_o) = \frac{V}{D} a C_o \tag{8.36}$$

Also:

$$\frac{\partial f_L}{\partial x} = \frac{\partial f_L}{\partial t}\frac{\partial t}{\partial x} = -\frac{1}{V}\frac{\partial f_L}{\partial t} \tag{8.37}$$

Substituting (8.36) and (8.37) in the solute balance equation:

$$\frac{\partial f_L}{f_L} = -\frac{\partial C_L}{C_L(1-k) + aC_o}$$

Upon integration between C_o and C_L, we obtain the local solute redistribution equation for dendritic solidification:

$$C_S = kC_o\left[\frac{a}{k-1} + \left(1 - \frac{ak}{k-1}\right)(1 - f_S)^{k-1}\right] \tag{8.38}$$

If $f_S(T)$ is known, the shape of the columnar dendrite can be calculated. The limits $a = 0$ and $a = -(1 - k)/k$ correspond to the condition of Scheil and equilibrium solidification, respectively. For an *Al*-4% *Cu* alloy a maximum of 9% eutectic is predicted to form in the interdendritic solidification for $a = 0$, and less for $a < 0$ (see Application 8.2).

The hemispherical approximation analysis of Burden and Hunt (1974), slightly modified by Laxmanan (1985) resulted in the following equation for tip undercooling:

$$\Delta T = \frac{D_L G_T}{V} - \frac{V m C_o (1-k) r}{D_L} - krG_T + \frac{2\gamma_{SL} T_L}{\rho_S \Delta H_f r} \tag{8.39}$$

Assuming further that growth proceeds at the *extremum*, that is $\partial(\Delta T)/\partial r = 0$, an equation for the tip radius of an array of instabilities as a function of the solidification velocity can be derived:

$$r = \sqrt{\frac{2\Gamma}{mC_o(k-1)V/D - kG_T}} = \sqrt{\frac{2\Gamma}{G_L - kG_T}}$$

When substituting this equation in Eq. (8.39) a $V(\Delta T)$ equation is obtained. The tip composition was calculated to be:

$$C_t = C_o\left(1 - a - \left(\frac{2\Gamma V(1-k)}{mD_L C_o}\right)^{1/2}\right)$$

8.4 Dendritic arm spacing and coarsening

The dendritic arm spacing (DAS) is a morphological parameter directly related to the mechanical properties of the alloy. In general, the finer is the arm spacing, the higher the mechanical properties. In columnar solidification, both primary and secondary arm spacing can be measured through metallographic analysis. In equiaxed solidification, only the secondary arm spacing is an issue. In the characterization of the fineness of the microstructure, the primary arm spacing is replaced by the number of grains.

8.4.1 Primary spacing

The relationship that allows calculation of the primary spacing, λ_1, is a complicated dependency of solidification velocity and temperature gradient. Two simpler relationships for the primary DAS will be discussed here.

A first relationship can be obtained based on *Flemings* array (Figure 8.13). Ignoring solute diffusion in the *x*-direction, material balance dictates:

$$D_L \frac{\partial^2 C_L}{\partial y^2} = \frac{\partial C_L}{\partial t} \quad \text{where} \quad \frac{dC_L}{dt} = \frac{dC}{dx}\frac{dx}{dt} = -\frac{V_y G_L}{m}$$

Upon substitution in the governing equation we have $\left(d^2C_L/dy^2\right) = -(V/D_L)(G/m)$. Integrating between 0 and *dC/dy*, and between 0 and *y* yields $dC/dy = -VGy/Dm$. Integrating again between C_o/k and C_L^{max} (in the interdendritic spacing), and between 0 and $\lambda/2$ gives:

$$\lambda^2 = -\frac{8mD}{VG}\left(C_L^{\max} - \frac{C_o}{k}\right) \quad \text{or}$$

$$\lambda_1 = ct.(GV)^{-1/2} \quad \text{or, more general,} \quad \lambda_1 = ct.\left(\dot{T}\right)^{-n} \tag{8.40}$$

Examples of cooling rates and dendrite arm spacing are given in Table 8.2.

Kurz and Fisher (1989) have derived a more complex relationship. Assume that the dendrites are half of ellipsoids of revolution (Figure 8.14). Then, the dendritic tip radius is $r = b^2/a$. For a hexagonal arrangement of dendrites $b = 0.58\lambda_1$. From the phase diagram it can be approximated that:

$$a = \frac{\Delta T'}{G} = \frac{T^* - T_E}{G} \approx \frac{\Delta T_o}{G}$$

Table 8.2. Range of cooling rates in solidification processes (Cohen and Flemings, 1985).

Cooling rate, K/s	Production processes	Dendrite arm spacing, μm
10^{-4} to 10^{-2}	large castings	5000 to 200
10^{-2} to 10^{3}	small castings, continuous castings, die castings, strip castings, coarse powder atomization	200 to 5
10^{3} to 10^{9}	fine powder atomization, melt spinning, spray deposition, electron beam or laser surface melting	5 to 0.05

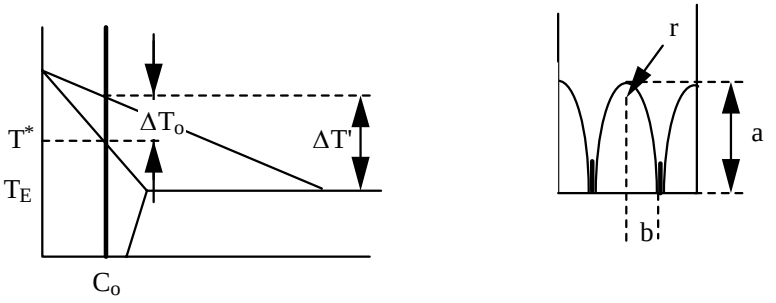

Figure 8.14. Assumptions for calculation of primary DAS (Kurz and Fisher, 1989).

This approximation is increasingly valid, as the composition of the alloy is closer to the eutectic. Then: $(0.58\lambda_1)^2 = r\,\Delta T_o / G$, or $\lambda_1 = \sqrt{3\Delta T_o r / G}$. Since $r = 2\pi\sqrt{D\Gamma/(V\,\Delta T_o)}$:

$$\lambda_1 = \mu_{\lambda 1} \cdot V^{-1/4} \cdot G^{-1/2} \quad \text{where} \quad \mu_{\lambda 1} = 4.3\left[\Delta T_o\, D_L\, \Gamma\right]^{1/4} \tag{8.41}$$

The constant refers to a single-phase alloy.

Earlier, Hunt (1979) has derived a similar equation for primary spacing different only through the numerical constant, which was 2.83 rather than 4.3. Note that all models introduced here demonstrate that the primary spacing is a function of G and V.

Bouchard and Kirkaldy (1997) tested these equations against experimental data for steady-state solidification of cells (28 alloys) and dendrites (21 alloys) in binary alloys. The experimental data summarized by the following equations agree reasonable well with theoretical predictions:

for cells: $\lambda_1 = ct. \cdot \dot{T}^{-0.36\pm0.05}$

for dendrites: $\lambda_1 = ct. \cdot V^{-0.28\pm0.04} \cdot G^{-0.42\pm0.04}$ and $\lambda_1 = ct. \cdot \dot{T}^{-0.3\pm0.03}$

However, for unsteady-state flow all equations failed to perform adequately.

Once the primary spacing is established, it will remain constant throughout steady - state solidification, and during cooling in solid state. If non-steady state solidification occurs, the primary spacing will change. Two typical mechanisms for adjustment of primary spacing are presented in Figure 8.15. Engulfing results in the increase of DAS while branching decreases DAS.

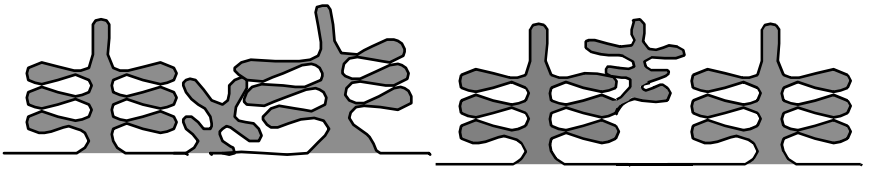

a) engulfing b) branching

Figure 8.15. Mechanisms for primary DAS adjustment.

8.4.2 Secondary arm spacing

In the early understanding of dendrite growth, it was assumed that the secondary dendrite arm spacing is formed at the beginning of solidification. Then, arms thicken and grow as solidification proceeds. Thus, the final arm spacing, λ_f, was thought to be the same as the initial spacing, λ_o.

Later it was realized that as solidification proceeds, only the larger arms grow. The smaller arms remelt (dissolve) and eventually disappear. Consequently, throughout solidification the secondary arm spacing (SDAS) increases and $\lambda_f > \lambda_o$. This is the dynamic coarsening of dendrites. The effect of coarsening on the SDAS of a transparent organic material is shown in Figure 7.16f. It is seen that the secondary DAS increases with the distance behind the tip.

Many mathematical models have been developed for dendrite coarsening based on the concept that dendrite coarsening is diffusion controlled, the diffusive species under consideration being the solvent. Assuming isothermal coarsening, the growth rate of the distance, λ, between two spherical particles must be proportional to the compositional gradient:

$$d\lambda/dt = ct \cdot (\Delta C_L/\lambda) \tag{8.42}$$

The liquid temperature and composition in equilibrium with a solid surface depends on the curvature of that surface. Indeed, the curvature undercooling at the tip of the dendrite is $\Delta T_r = 2\Gamma/r$. Since $\Delta T_r = m\,\Delta C_r$, $\Delta C_r = 2\Gamma/(m\,r) = ct \cdot r^{-1}$. Curvature and local curvature differences must increase approximately proportionally with the inverse of the spacing λ. Thus. $r = ct{\cdot}\lambda$. It follows that $\Delta C_r = ct{\cdot}\lambda^{-1}$, and also $\Delta C_L = C_{r1} - C_{r2} = ct \cdot \lambda^{-1}$.

Substituting in Eq. (8.42) yields $d\lambda/dt = ct{\cdot}\lambda^{-2}$. Rearranging and integrating between an initial arm spacing, λ_o, and λ_f, and between zero and the final local solidification time (the difference between the times when the liquidus isotherm and the solidus isotherm pass the particular microvolume), t_f, gives:

$$\lambda_f^3 - \lambda_o^3 = \mu_o \cdot t_f \tag{8.43}$$

Assuming that $\lambda_o << \lambda_f = \lambda_2$, results in a final secondary arm spacing of:

$$\lambda_2 = \mu_o^{1/3} \cdot t_f^{1/3} \tag{8.44}$$

where t_f is the local solidification time.

Using the experimental data presented Figure 8.16 it can be calculated that, for Al-4.5% Cu alloys, the constant in the coarsening law has a value of 10^{-16} m/s^3.

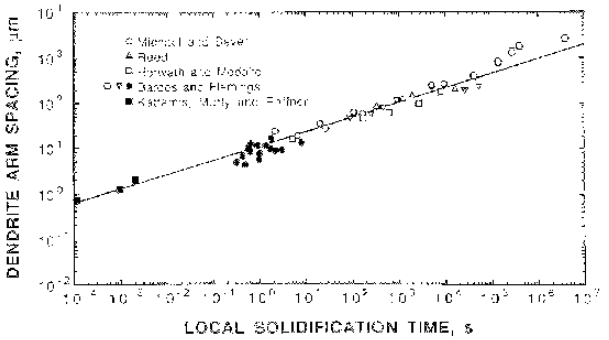

Figure 8.16. Relation between SDAS and solidification time for Al-4.5% Cu alloys (Flemings *et al*., 1991). Copyright 1991 American Foundry Soc., used with permission.

The constant in Eq. (8.44) has been derived by a number of authors, mostly for the case of spherical particles (see for example the derivation in the inset). Some typical formulations and their basic assumptions are given in Table 8.3. Isothermal coarsening assumes that the only driving force is solute diffusion and that the fraction solid is constant. However, during solidification the temperature decreases, the fraction solid increases, and an additional driving force, thermal diffusion, must be considered. This is dynamic coarsening.

Table 8.3. Coarsening constants.

Model	Coarsening constant	Basic assumptions
Kattamis-Flemings, 1965	$\mu_o = \dfrac{20 D_L \Gamma \ln(C_E/C_o)}{m_L C_L (k-1)(C_E - C_o)}$	isothermal coarsening, of spheres; see inset for derivation
Ardell, 1972	$\mu_o = \dfrac{v_m^2 \gamma_{SL} C_o D_L}{RT}(1-C_o)\dfrac{1-f}{f}$ C_o in fraction	dynamic coarsening of spheres, diffusion of solute depends on a characteristic distance defined by the main free path
Voorhees-Glicksman, 1984	$\mu_o = \dfrac{8}{9}\dfrac{v_m^2 \gamma_{SL} C_o D_L}{RT}\dfrac{\alpha^3}{1-f^{1/3}}$ α: fct. of f_S given in tabulated form	solution of dynamic multiparticle diffusion problem; random pattern of precipitates generated by Monte Carlo simulation
Mortensen, 1991	$\mu_o = \dfrac{27 D_L \Gamma}{2 m_L C_L (k-1) f_S^{2/3}(1-f_S^{1/3})}$	dynamic coarsening of spheres
	$\mu_o = \dfrac{27 D_L \Gamma}{4 m_L C_L (k-1) f_S (1-f_S^{1/2})}$	dynamic coarsening of cylinders

Derivation of coarsening constant - Kattamis/Flemings model.
The basic assumptions of the model are as follows: isotropic growth of two spherical dispersoids of constant total volume; constant concentration gradient; unidirectional diffusion; the radius of the larger dispersoid is much larger than that of the smaller dispersoid ($r_2 >> r_1$).

Both spheres are at the same undercooling and separated by a distance λ. As discussed before, the difference in the interface concentration of the two spheres is:

$$\Delta C = C_L^{r_2} - C_L^{r_1} = \frac{\Gamma}{m}\left(\frac{1}{r_1} - \frac{1}{r_2}\right)$$

The flux of solute from r_2 to $r_1$is: $$J = -D\frac{\Delta C}{\lambda} = -\frac{D\Gamma}{\lambda m}\left(\frac{1}{r_1} - \frac{1}{r_2}\right)$$

The flux of solvent from r_1 to r_2 is: $$J = \left(\left(1 - C_L^{r_1}\right) - \left(1 - C_S\right)\right)\frac{dr}{dt} = -C_L^{r_1}(1-k)\frac{dr}{dt}$$

Flux balance gives: $$\frac{dr}{dt} = \frac{D\Gamma}{m C_L^{r_1}(1-k)\lambda}\left(\frac{1}{r_1} - \frac{1}{r_2}\right)$$

It is further assumed that the interface concentration of the large particle is equal to the average liquid concentration due to segregation, $C_L^{r_1} \approx C_L$, and that the liquid concentration is a linear function of time, from an initial concentration C_o to the final eutectic concentration C_E:

$$C_L = C_o + (C_E - C_o)\frac{t}{t_f}$$

If it is also assumed that since $r_2 >> r_1$, r_2 = ct. and r_1 = f(r), the last equation can be integrated between the initial time (0) when the small particle has a radius $r_1 = r_o$, and the time tf when the particle has vanished:

$$\int_{r_1=r_o}^{0} \frac{r_1 r_2}{r_2 - r_1} dr = \int_0^{t_f} \frac{D\Gamma}{mC_L(1-k)\lambda} dt$$

The final coarsening time is then: $t_f = \frac{mC_L(k-1)(C_E - C_o)}{D\Gamma \ln(C_E/C_o)} \lambda r_2^2 \left(\frac{r_o}{r_2} + \ln\left(1 - \frac{r_o}{r_2}\right) \right)$

It is not surprising that the coarsening time depends on the initial size of the particles. To obtain an order of magnitude of the coarsening constant it can be further assumed that $r_2 = 0.5\lambda$ and $r_o = 0.5\, r_2$. Then:

$$\lambda_f^3 = \frac{20 D_L \Gamma \ln(C_E/C_o)}{m_L C_L (k-1)(C_E - C_o)} t_f$$

The majority of models for the temporal evolution of λ_2 assume that the dendrite arms have a cylindrical shape (*e.g.* Kattamis *et al*. 1967). Calculations then predict the axial remelting of the thinner arm.

Other models consider the dendrite arms to be tear-shaped. If a tear-shaped arm is surrounded by two cylindrical arms (Chernov, 1956) material is transported from the base where the radius of curvature r_1 is small, to the tip, where the radius r_2 is large (Figure 8.17a). Eventually r_2 becomes zero and the arm detaches from the stem of the dendrite as demonstrated experimentally by Papapetrou (1935) (see Figure 8.18).

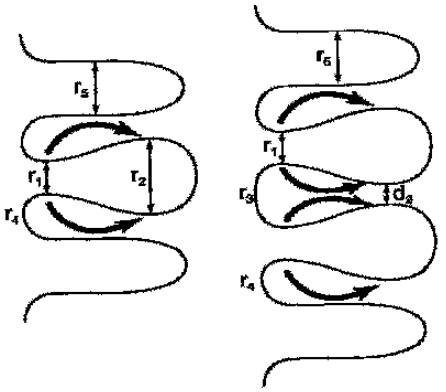

Figure 8.17. Material transport for (a) one tear-shaped arm surrounded by cylindrical arms, or (b) two tear-shaped arms surrounded by cylindrical arms (Mendoza *et a*l. 2003). With kind permission of Springer Science and Business Media.

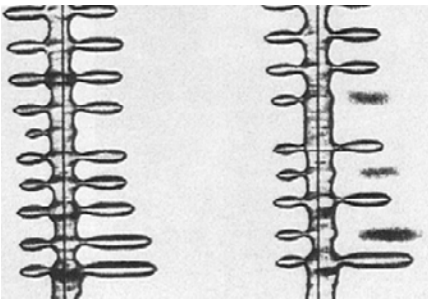

Figure 8.18. Separation of dendrite arms in NH4Cl (Papapetrou, 1935). After separation the detached arms move out of focus.

If case (b) in Figure 8.17 is considered (Young and Kirkwood, 1975), material transported away from the base accumulates at the tip and the distance d_2 decreases until coalescence occurs. Experimental evidence of this mechanism is shown in Figure 8.19.

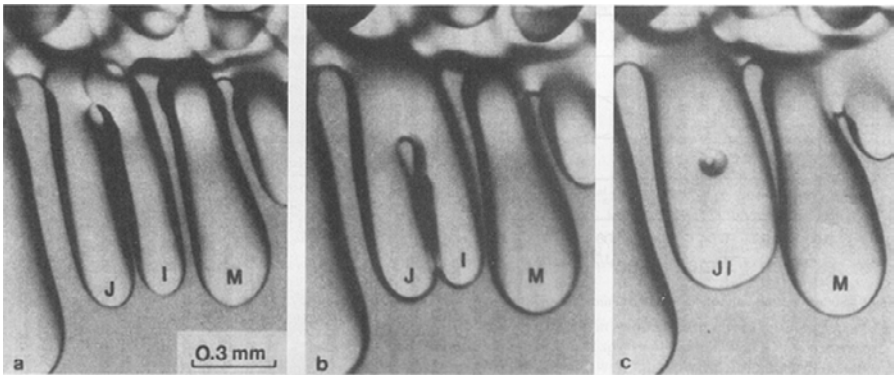

Figure 8.19. Coalescence of arms J and I in succinonitrile (Huang and Glicksman, 1981). Reprinted with permission from Elsevier.

Experimental data on secondary arm spacing have also been reported to fit an equation similar to Eq. (8.40) proposed for primary spacing. Analysis of 60 experimental data on two alloys by Bouchard and Kirkaldy (1997) produced the following relationship:

$$\lambda_2 = ct \cdot \left(\dot{T}\right)^{-0.34\pm0.02}$$

For alloys solidifying with equiaxed structure, it is not possible to define a primary arm spacing. To evaluate the length scale of the microstructure the average grain size (average diameter of grains on the metallographic sample), or volumetric grain density (number of grains per unit volume) are used. These numbers are primarily functions of the nucleation potential of the melt. Secondary arm spacing can also be used to evaluate the fineness of equiaxed structures. However, as noted above, it represents thermal conditions during solidification, not nucleation conditions. Thus, it is possible to have a coarse grained casting with fine secondary arm spacing.

8.5 The columnar-to-equiaxed transition

In many applications, either a columnar or an equiaxed structure is desired for the casting. If, because of lack of adequate process control, a sudden columnar-to-equiaxed transition (CET) occurs in these castings, they will be rejected having an unacceptable structure. Therefore, it is important to understand the conditions under which a CET can occur in a given casting.

An example of such a transition in an ingot is shown on Figure 8.20. This is not a schematic drawing but a modeled microstructure, which correctly describes the real microstructure. The details of the model will be discussed in Section 13.1.1. The results of the calculations are very realistic. Three different structural regions are shown on the middle ingot: a chill zone, made of small equiaxed grains result-

ing from rapid cooling against the mold wall; a columnar zone; an equiaxed zone toward the middle of the casting. The figure also indicates that as the undercooling increases the structure in the bulk of the ingot changes from fully columnar to mixed columnar /equiaxed. Thus, a CET occurs as the undercooling is increased. A typical structure showing the CET in an Al-5%Cu ingot is presented in Figure 8.21. One possible rationalization of the occurrence of CET is in terms of constitutional undercooling. At the beginning of solidification, the temperature gradient in the liquid is rather high, and constitutional undercooling is limited (Figure 8.22a). As solidification continues, the mold is heated. The temperature gradient in the liquid decreases and the constitutional undercooling may reach the middle of the casting (Figure 8.22b). If nucleation of equiaxed grains occurs they will have favorable conditions and will grow ahead of the columnar interface (see also Figure 7.13).

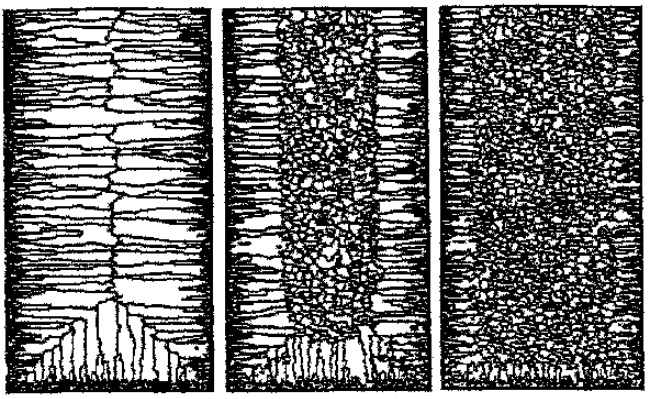

Figure 8.20. Typical structural regions in castings (Zhu and Smith, 1992). Reprinted with permission from Elsevier.

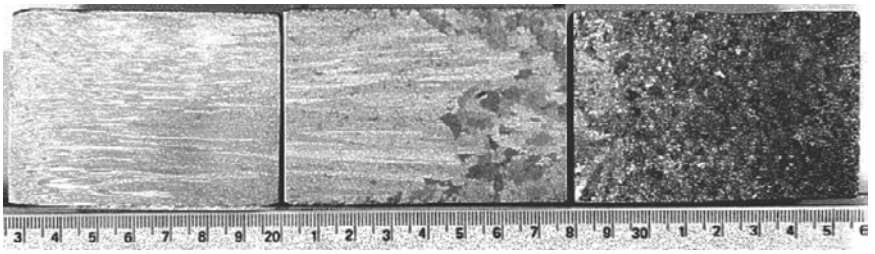

Figure 8.21. CET occurring in an Al-5 wt% Cu ingot solidified against a chill placed at its base (Guo and Stefanescu, 1992). Solidification is from right-to-left. The CET occurred when the temperature gradient in the melt ahead of the interface decreased in the range of 113 to 234K/m. In the equiaxed zone the number of grains was $5 \cdot 10^{6} m^{-3}$. The average solidification velocity at the CET was measured to be $3.5 \cdot 10^{-4} m/s$. Copyright 1992 American Foundry Soc., used with permission.

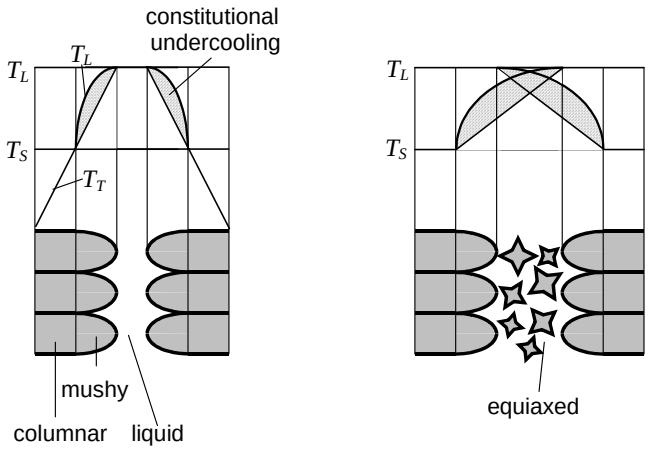

a) no constitutional undercooling in the middle of the casting - only columnar growth is possible

b) constitutional undercooling in the middle of the casting - if nucleation occurs, equiaxed growth is possible

Figure 8.22. Occurrence of CET because of increased constitutional undercooling resulting from lower temperature gradient.

While the role of constitutional undercooling in the CET is not under dispute, it does not seem to be the only mechanism responsible for it. Chalmers (1962) has shown that when the center of a casting is isolated with a cylinder, fewer and coarser grains grow than in the absence of isolation. This is in spite of the fact that the center is constitutionally undercooled in both cases. Chalmers then proposed the "*Big Bang Mechanism*" which postulates that equiaxed grains result from the nuclei formed during pouring by the initial chilling action of the mold. The grains are then carried into the bulk liquid. If they survive until the superheating is removed a CET occurs. However, assuming that only the big bang is responsible for CET cannot account for equiaxed zone formation in the absence of a chilled mold.

Jackson *et al.* (1966) noticed that increased convection during solidification of organic alloys produced a large number of nuclei in the liquid. They postulated that dendrite arms remelt because of recalescence, detach from the dendrite stem and then float into the center of the casting where they serve as nuclei for equiaxed grains. Another argument for the *dendrite detachment mechanism* is that the mechanical strength of the dendrite is negligible close to its melting point, and thus convection currents can simply break the dendrite (O'Hara and Tiller, 1967).

Hunt (1984) has proposed a 1D analytical model for the CET based on the following assumptions: equiaxed grains are formed by heterogeneous nucleation and do not move with the liquid, steady state is possible for a fully columnar, columnar + equiaxed, or fully equiaxed growth. It was further assumed that a fully equiaxed structure results when the fraction of equiaxed grains is higher than a critical fraction of solid, $f_S^e > f_S^{cr} = 0.49$, and that a fully columnar structure is produced when $f_S^c < 10^{-2}\, f_S^{cr} = 0.0049$. Using a model of hemispherical dendrite growth, and assuming small thermal undercooling the following criteria were derived:

- fully equiaxed growth occurs when:

$$G_T < 0.49\left(\frac{N}{f_S^{cr}}\right)^{1/3}\left[1-\frac{(\Delta T_N)^3}{(\Delta T_c)^3}\right]\Delta T_c \tag{8.45a}$$

- fully columnar growth develops when:

$$G_T > 0.49\left(\frac{100\cdot N}{f_S^{cr}}\right)^{1/3}\left[1-\frac{(\Delta T_N)^3}{(\Delta T_c)^3}\right]\Delta T_c \tag{8.45b}$$

where N is the volumetric nuclei density, ΔT_N is the undercooling required for heterogeneous nucleation, and ΔT_c is the undercooling at the columnar front calculated as:

$$\Delta T_c = \left[-8\Gamma m_L(1-k)C_o V/D\right]^{1/2} \tag{8.46}$$

The selection of the thresholds in the derivation of the above relationships is debatable. It seems difficult to accept that columnar grains can grow beyond the point when dendrite coherency is established, f_S^{coh}. Accordingly, a more reasonable upper limit is $f_S^{cr} = f_S^{coh}$. Typically f_S^{coh} = 0.2-0.4. Also, mixed equiaxed-columnar structures are seldom observed in castings. In most cases an abrupt CET is seen. Indeed, microgravity work performed by Dupouy *et al*. (1998) on Al-4% Cu alloys demonstrated that while a smooth (mixed structure) CET is obtained in microgravity (no thermo-solutal convection), an abrupt CET is seen on the same sample solidified under terrestrial conditions. Thus, it is reasonable to assume that the CET occurs simply when coherency is reached.

Another weak assumption is that of stationary equiaxed grains. Indeed, because of the thermo-solutal and shrinkage convection, the equiaxed grains will move with the liquid, unless coherency is reached. As discussed previously, one of the main reasons for the CET is the presence of thermosolutal convection.

Based on the preceding discussion a new model is proposed in the following paragraphs. Consider a volume element of length l, that extends from some arbitrary point in the columnar region to a region where the temperature is equal to the nucleation temperature, ΔT_N that is very close to the liquidus temperature (Figure 8.23). Consequently, the grains moving away out of the volume element in the bulk liquid in the x-direction will not survive, and no grains are advected from the bulk liquid into the element in the x-direction. It is further assumed that the net contribution of the flow in the y-direction to the number of grains is zero. Within the volume element the CET occurs if the equiaxed grains can reach f_S^{coh} before the columnar front traverses the element. Thus, condition for the CET is:

$$t_c \geq t_e^{coh} \tag{8.47}$$

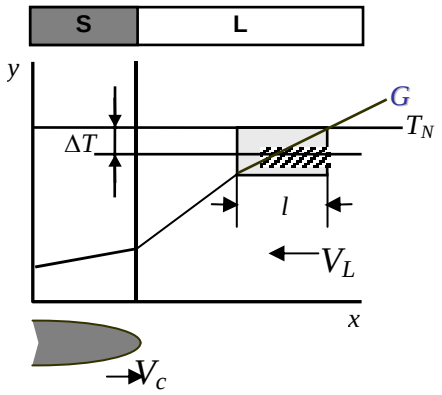

Figure 8.23. Volume element for calculation of CET.

where t_c is the time required for the columnar front to move across the volume element, and t_e^{coh} is the time required for the equiaxed grains to reach coherency. Then:

$$t_c = l/V_c = 2\Delta T/(GV_c) = 2\Delta T/(G\mu_c \Delta T^2)$$

where G and ΔT are the average thermal gradient and undercooling in the volume element, respectively, V_c is the growth velocity of the columnar dendrites, and μ_c is the growth coefficient of the columnar dendrites.
Similarly, since when assuming spherical grains, the fraction of solid in the volume element can be calculated as $f_S = (4/3)\pi \bar{r}^3 \overline{N}$, where $\bar{r}$ and $\overline{N}$ are the average grain radius and the average volumetric grain density, respectively:

$$t_e^{coh} = \frac{\bar{r}^{coh}}{V_e} = \left(\frac{3}{4\pi}\frac{f_S^{coh}}{\overline{N}}\right)^{1/3} \left(\mu_e \Delta T^2\right)^{-1}$$

where V_e is the growth velocity of the equiaxed dendrites, and μ_e is the growth coefficient of the equiaxed dendrites.

Introducing the last two equations the CET criterion Eq. (8.47), the CET will occur when:

$$G_T \leq 3.22\left(\frac{\overline{N}}{f_S^{coh}}\right)^{1/3} \frac{\mu_e}{\mu_c}\Delta T \tag{8.48}$$

In turn, the average volumetric grain density can be written as the difference between the active heterogeneous nuclei, N, and the grains entering the volume element because of fluid flow into the volume element:

$$\overline{\overline{N}} = N + (V_L / V)N$$

where V_L is the flow velocity in the x-direction, and V is the solidification velocity. Note that if $V_L = V$, $\overline{\overline{N}}$ =0, and equiaxed solidification is impossible. Substituting in Eq. (8.48) the final CET condition becomes:

$$G_T \leq 3.22\left[\frac{\overline{\overline{N}}}{f_S^{coh}}\left(1+\frac{V_L}{V}\right)\right]^{1/3}\frac{\mu_e}{\mu_c}\Delta T \tag{8.49}$$

This equation suggests that the probability of formation of an equiaxed structure increases as the nucleation potential, and the undercooling increase, and as the coherency solid fraction and liquid convection decrease. Note that for the case when convection is ignored (V_L = 0), this equation is very similar to those derived by Hunt. However, it was obtained using less restrictive assumptions.

This model could be further developed to include grain transport into the volume element, by assuming that the outer limit of the element is at a temperature below the nucleation temperature, or if the number of grains to be advected in the volume element can be calculated.

8.6 Applications

Application 8.1

Compare the solutal and thermal undercooling for an Al-4.5% Cu alloy and for an Fe-0.09% C alloy.

Answer:
Since the expressions for undercooling include both velocity and tip radius it is not possible to calculate the undercooling without additional data. However, a comparison can be made by calculating the ratio $\Delta T/Vr$ for the two cases. From Eqs.(8.7)) and (8.6a), and using data in Appendix B:

$\Delta T_c / Vr = m(k-1)C_o / 2kD$ = $1.03 \cdot 10^{10}$ K·s·m^{-2} for the Al-Cu alloy, and = $8.9 \cdot 10^{8}$ K·s·m^{-2} for the Fe-C alloy

$\Delta T_T / Vr = \Delta H_f / 2\alpha c$ = $4.94 \cdot 10^{6}$ K·s·m^{-2} for the Al-Cu alloy, and = $2.53 \cdot 10^{7}$ K·s·m^{-2} for the Fe-C alloy

It is obvious that the thermal undercooling is very small as compared with the solutal undercooling for the Al-Cu alloy, but within an order of magnitude for the Fe-C alloy. Thus, the thermal undercooling cannot always be neglected.

Application 8.2

Compare the tip radius - growth velocity correlation for solutal dendrites and solutal-thermal dendrites for a Fe-0.09% C alloy using the Nastac-Stefanescu (NS) (1993) and the Trivedi-Kurz TK (1994) models.

Answer:
Combining Eqs. (8.23) and (8.24) and assuming steady-state, we obtain the *V-r* correlation for the NS model as follows:

$$V r^2 = 8\pi^2 \Gamma \left(\frac{m(k-1)C_o}{k D_L} + \frac{\Delta H_f}{c \alpha_L} \right)^{-1} \tag{8.50}$$

For the TK model, assuming steady-state and low Péclet number (<<1) we can obtain a similar equation from Eq. (8.19):

$$V r^2 = 4\pi^2 \Gamma \left(\frac{m(k-1)C_o}{D_L} + \frac{\Delta H_f}{2 c_L \alpha_L} \right)^{-1} \tag{8.51}$$

For the solutal dendrite, that is a dendrite whose growth is controlled solely by the solutal field, only the first term in the parenthesis is used. Using data in Appendix B we obtain the graph in Figure 8.24. It is seen that there is no difference between the solutal NS and TK in the range of velocities used in the calculation. When the effects of thermal undercooling are also used in the NS model, a slight decrease in tip radius is calculated.

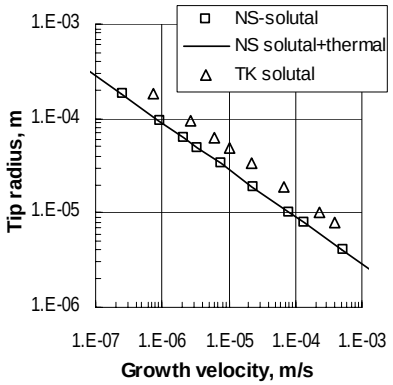

Figure 8.24. Calculated dendrite tip radii for solutal and solutal-thermal dendrites for a Fe-0.09% alloy.

Application 8.3

Compare the dendrite tip radius - growth velocity relationship calculated with the Trivedi-Kurz (1994) and Nastac-Stefanescu (1993) models, with the experimental data on the Fe-3.08% C-2.01% Si - 0.104% Mn - 0.016% S - 0.029% P alloys obtained by Tian and Stefanescu (1992).

Answer:
For the NS model the solutal part of Eq. (8.50) will be used. For the TK model the model for columnar dendrite, Eq. (8.21), will be used. Again, assuming steady state ($C_L^* = C_o/k$) and low Péclet number (ξ_c = 1) the TK columnar dendrite growth velocity becomes:

$$V = \left(\frac{4\pi^2 \Gamma}{r^2} + G_T \right) \frac{D_L}{m(k-1)C_o} \tag{8.52}$$

Since the alloy is a multicomponent alloy, the average composition C_o must be expressed as a carbon equivalent to reduce the multicomponent alloy to a binary one. The following relationship is used:

$$C_o = \%C + 0.31 \bullet \%Si + 0.33 \bullet \%P - 0.27 \bullet \%Mn + 0.4 \bullet \%S = 3.72$$

The predicted and experimental results are plotted in Figure 8.10. Note that while the NS model fails at growth velocities smaller than ~1μm/s, it describes growth reasonable well within the range of velocities typical for castings. It is also the simplest one to implement in a numerical code. The thermal gradient is important only in the cellular solidification range.

Application 8.4

Calculate the amount of eutectic that will solidify in the interdendritic regions of an Al-4% Cu alloy, for three different solidification velocities: $3 \cdot 10^{-5}$, $1 \cdot 10^{-7}$, $6 \cdot 10^{-8}$ m/s. Assume a constant temperature gradient of 2000 K/m.

Answer:
The required materials constant are obtained from Appendix B and listed in the Excel spreadsheet in column A. The maximum solubility of Cu in Al is 5.65%. When the composition reaches this value the rest of the liquid solidifies as eutectic.

The calculation of the solid composition is performed in columns D, E, and F based on the fraction solid listed in column C (Table 8.4). First the parameter a is calculated for the three velocities. Cells D3, E3, and F3 include the equation for a, *i.e.*, Eq. (8.35). Columns D, E, and F starting with cells D6, E6, and F6 include the equation for C_S, i.e. Eq. (8.38). The calculation is run until $C_S = 5.65$.

Table 8.4. Organization of spreadsheet.

	A	B	C	D	E	F
1	Constants	Data				
2	D_L	2.8E-9	V	3.00E-05	1.00E-07	6.00E-08
3	G_L	2000	a	-1.15E-02	-3.46E+00	-5.76E+00
4	m	-3.6				
5	C_o	4.5	f_S	C_S	C_S	C_S
6	k	0.14	0	0.64	2.81	4.26
7	C_{max}	5.65	0.1	0.70	2.83	4.26
8			0.2	0.77	2.87	4.27
9			0.3	0.86	2.91	4.27
10			0.915	5.25	4.83	4.55
11			0.922	5.65	5.00	4.57
12			0.9405		5.65	4.66
13			0.9845			5.63

The calculation results are shown in Figure 8.25. The fraction of eutectic is calculated as $f_E = 1 - f_S$. It is seen that for $V = 3 \cdot 10^{-5}$, for which a is very small, the calculated fraction of eutectic is 0.078. As V increases to $1 \cdot 10^{-7}$, f_E decreases to 0.059, and to 0.016 for $V = 6 \cdot 10^{-8}$. It

will become zero for equilibrium solidification when the velocity is so small that $a = (k - 1)/k$.

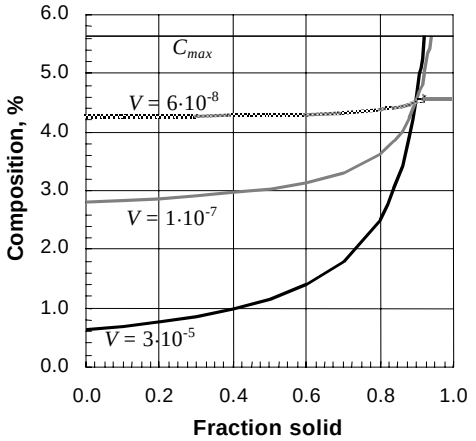

Figure 8.25. Calculation of amount of eutectic as a function of solidification velocity.

Application 8.5

Calculate the temperature and solid fraction evolution during the solidification of an equiaxed dendrite of an Fe-0.6%C alloy that has a volumetric grain density of 1 grain/mm^3. Assume that the alloy is cooled at constant heat extraction rate of $\dot{Q}$ =3·10^8 J·m^{-3}·s^{-1}, and an initial temperature of 1520°C.

Answer:
The governing heat transport equation is: $\dot{Q} = \rho \Delta H_f \, df_S / dt - \rho c dT / dt$. Rearranging and discretizing for time-stepping:

$$T^{new} = T^{old} - \frac{\dot{Q}}{\rho c} \Delta t + \frac{\Delta H_f}{c} \Delta f_S^{new} \tag{a}$$

Note that this equation is independent of volume. Assuming a spherical equiaxed dendrite, $f_S = (4/3)\ \pi\ r_S^3\ N$, and $df_S / dt = 4\pi\, r_S^2\ N\, dr_S / dt = 4\pi\, r_S^2\ N\, V_S$. The number of nuclei, N, is equal to one. The time-discretized equation is:

$$\Delta f_S^{new} = 4\,\pi \left(r_S^{new} \right)^2 V_S^{new} \Delta t \tag{b}$$

Further, the grain size is:

$$r_S^{new} = r_S^{old} + V_S^{ewn} \Delta t \tag{c}$$

The solidification velocity is $V_S = \mu \cdot \Delta T^2$. The growth coefficient can be calculated with Eq. (8.22). Assuming a solutal dendrite, the discretized equation for the solidification velocity is:

$$V_S^{new} = \frac{D_L}{2\pi^2 \Gamma m(k-1)\langle C_L \rangle^{new}} \left(\Delta T^{new}\right)^2 \quad \text{(d)}$$

where $\langle C_L \rangle$ is the average liquid composition.

To calculate the average liquid composition needed in this equation, a diffusion model must be used. We will compare the Scheil and equilibrium diffusion models. The time discretized equations for the two models are:

Scheil: $C_L^{new} = C_o\,(1 - f_S^{old})^{k-1}$ Equilibrium: $C_L^{new} = \frac{C_o}{1-(1-k)\,f_S^{old}}$ (e)

The evolution of the fraction solid is: $f_S^{new} = f_S^{old} + \Delta f_S^{new}$ (f)

Finally, the undercooling is calculated as:

$$\Delta T = \Delta T_c + \Delta T_T = m(C_o - C_L) + T^* - T_{bulk} = T_f + mC_o - T_{bulk}$$

where T_{bulk} is the average temperature in the volume element (the macro-temperature). C_o is the average liquid composition, $\langle C_L \rangle$. In discretized form this is:

$$\Delta T^{new} = T_f + m\langle C_L \rangle^{new} - T^{old} \quad \text{(g)}$$

Table 8.5. Program implementation on the Excel spreadsheet.

time	$\langle C_L \rangle$	ΔT	V_S	r_S	Δf_S	f_S	T
Eq.	(e)	(g)	(d)	(c)	(b)	(f)	(a)
0				1.00E-07			1520
0.01	0.600	00	0.00E+00	1.00E-07	0.00E+00	0.00	1519.5
0.59	0.6	0.394	2.62E-05	3.62E-07	4.31E-19	4.31E-19	1489.1
1.47	0.602	44.7	3.35E-01	1.07E-01	4.82E-04	0.01	1444.8
4.63	0.891	19.4	4.29E-02	4.90E-01	1.29E-03	0.50	1447.2
9.17	1.746	17.6	1.79E-02	6.19E-01	8.62E-04	1.00	1380.5

Since above the liquidus temperature there is no undercooling, an IF statement must be included which allows this equation to become effective only at $T^{new} < T_L$. These equations are then implemented in the Excel spreadsheet, for example as shown in Table 8.5 fro the case of equilibrium. An initial radius at time zero is assumed. The initial temperature is 1520°C.

The calculated results are plotted in the Figure 8.26. It is seen that significant differences exist in both temperature and solid fraction evolution as a function of the chosen diffusion model. When the *Scheil* model is used, longer time is needed for completion of solidification, and a lower solidus temperature is reached (1187°C as compared to 1381°C for equilibrium). Dendritic solidification ends when the liquid composition becomes $C_L = C_E = 4.26$.

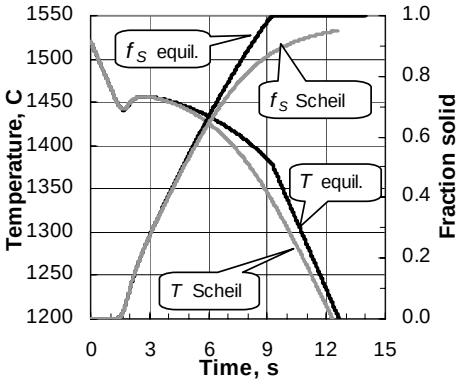

Figure 8.26. Evolution of temperature and solid fraction during the solidification of a condensed dendrite.

Application 8.6

Calculate the critical gradient for CET in the Al-5% Cu ingot presented in Figure 8.21 (N = $5{\cdot}10^6$ m^{-3} and V = $3.5{\cdot}10^{-4}$ m/s). Assume f_S^{coh} = 0.3. The other data required for calculation are given in Appendix B.

Answer:

Let us use the Hunt model first. From Eq. (8.46)) it is calculated that ΔT_c = 1.93K. Then, assuming that $\Delta T_N << \Delta T_c$ (which is not necessarily true), and using Eq. (8.45a) it is calculated that the critical gradient for CET is G_T = 205K/m for the f_S^{cr} = 0.49 postulated but Hunt. This is within the range determined experimentally, which was 113 to 234 K/m.

Let us now use the model described by Eq. (8.49). The steady-state growth coefficient for columnar growth can be calculated from Eq. (8.26)) as $\mu_c D_L \left(\pi^2 \Gamma m(k-1)C_o\right)^{-1}$. We obtain μ_c = $7.64{\cdot}10^{-5}$. Then, from the same equation, assuming that all undercooling is constitutional, the undercooling is ΔT = $\sqrt{V/\mu}$ = 2.14 K. The growth coefficient for the equiaxed grains can be calculated with Eq. (8.22). When the thermal undercooling is ignored we obtain μ_e = $5.35{\cdot}10^{-5}$. Introducing these values in Eq. (8.49**)**, it is obtained that G_T = 123 K/m, which is in range of the experimental data.

References

Akamatsu S., G. Faivre, and Th. Ihle, 1995, *Phys. Rev*. **E51**:4751–4773

Ananth R. and Gill W.N., 1988, *J. Crystal Growth* **91**:587

Ardell A.J., 1972, *Acta Metall*. **20**:61

Barbieri A. and Langer J.S., 1989, *Physical Review A* **10**:5314-5325

Bensimon D., Pelce P., and Shraiman B. I., 1987, *J. Phys. A* **48**:2081

Biloni H. and Boettinger W.J., 1996, in: *Physical Metallurgy*; fourth edition, R.W. Cahn and P. Haasen eds., Elsevier Science BV p.670

Boettinger W. J., Coriell S.R., and Trivedi R., 1988, in: *Rapid Solidification Processing: Principles and Technologies*, R. Mehrabian and P.A. Parrish eds., Claitor's Publishing, Baton Rouge, LA p.13

Bouchard D. and Kirkaldy J.S., 1997, *Metall. and Mater. Trans.* **28B**:651

Bowers T.F., Brody H.D. and. Flemings M.C, 1966, *Trans. AIME* **236**:624